Thermal Imaging of RF Induced Heat Loss in a Microwave Metamaterial Absorber

K. Ozden[1], **O. M. Yucedag**[2], **A. Ozer**[2], **H. Bayrak**[2], **H. Isik**[3], **and H. Kocer**[2]

[1]Defense Sciences Institute, Turkish Military Academy Ankara, Turkey
[2]Department of Electrical Engineering, Turkish Military Academy Ankara, Turkey
[3]Department of Mechanical Engineering, Turkish Military Academy Ankara, Turkey

Abstract— Metamaterial absorbers (MAs) play an important role in stealth technology in microwave bands. Although MAs absorb incident RF power, they usually convert it into the heat which might be a disadvantage for counter-measurement against remote thermal imaging systems. In this study, we present the design, simulation, fabrication and RF/thermal imaging of a narrowband MA in the microwave region. The MA consists of a two dimensional periodic array of a well-known metallic split ring resonator (SRR) and a ground plane separated by a dielectric layer. For horizontally and vertically polarized illumination cases, thermal imaging of the MA is carried out using a commercial thermal imager which has a longwave infrared sensor between 8–12 μm wavelengths. Surface temperature map of the MAs are extracted from the recorded thermal images. It is shown that a slight temperature difference happens with respect to the ambient temperature for the MA of the near-perfect absorption whereas the MA of the near-zero absorption has zero temperature difference. Physical mechanisms of the RF absorption and the RF induced heat loss are explained using further electromagnetic numerical simulations.

1. INTRODUCTION

Metamaterials are manmade structures which have novel features such as backward wave propagation, negative refractive index and phase velocity. Metamaterials with these properties are used in many practical applications such as super lenses [1], antennas [2], sensors [3] and perfect absorbers [4, 5]. The matematerial based perfect absorbers have attracted a great deal of interest in stealth technology in recent years. Metamaterial absorbers (MAs) consist of periodic conductive and insulator layers which are responsible for producing negative permittivity (ε) and permeability (μ) at resonance frequency. These artificial structures can be utilized as a radar absorbing material (RAM) in microwave bands.

Although metamaterials were theoretically investigated by a Russian physicist V. Veselago in 1968 [6], studies on MAs are not going too far back. The first metamaterial based absorption experiments were held by Landy et al. [4] in 2008. Initially, narrow bandwith perfect absorption was achieved. After that, most of the researches were concentrated on obtaining the polarization-insensitive [7], wide-angle [8], multi-band [9] and broadband absorption [10] using the MAs.

In this study, we present the design, simulation, fabrication and RF/thermal imaging of a narrowband-polarization sensitive MA in the microwave region. The MA consists of a two dimensional periodic array of a well-known metallic split ring resonator (SRR) proposed by Pendry et al. [11] and a ground plane separated by a dielectric layer. By adjusting the dimensions, the SRR is optimized to have resonance at 4.75 GHz. Measurements of the MA was held in uncontrolled room. It is observed that the RF simulation results are in good agreement with the measurements such that near-perfect absorption occurs at 4.75 GHz when the incident electric field vector is perpendicular to the SRR gaps. On the other hand, near-zero absorption is obtained when the incident electric field vector is parallel to the gaps. To better understand the mechanism of the RF absorption, the electric field distribution, magnetic field distribution and current distribution are simulated at on-resonance (4.75 GHz) and off-resonance (4.00 GHz) frequencies. It is seen that MA absorbs incident RF power at resonance frequency. The incident RF power is neither reflected nor transmitted but is turned into heat and get absorbed. While it might be an advantage to use MAs against microwave radars, it might be a disadvantage for counter-measurement against remote thermal imaging systems in infrared region. So, thermal imaging of the MA is carried out using a commercial thermal imager which has a longwave infrared sensor between 8-12 μm wavelengths. Surface temperature map of the MA is extracted from the recorded thermal images. It is shown that a slight temperature difference occurs for the MA of the near-perfect absorption whereas the MA of the near-zero absorption case has zero temperature difference.

2. DESIGN, SIMULATION AND MEASUREMENT OF THE METAMATERIAL ABSORBER

The proposed MA consists of two metallic layers separated by dielectric. The first metallic layer is the SRR and the second one is metallic continuous ground plane. The SRR consists of two concentric rings separated by a gap. A schematic drawing of the SRR can be seen in Fig. 1(a). Both rings have splits at the opposite sides. These metallic layers are selected as copper which has 35 μm thickness and its frequency independent conductivity (σ) is 5.8×10^7 S/m. The dielectric material is epoxy glass cloth laminate (FR4) which has 1.6 mm thickness and its relative dielectric permittivity (ε_r) is 3.85 and the loss tangent ($\tan\delta$) is 0.02. The geometrical parameters of the SRR are defined as follows: L is the length and width of the unit cell, d is the width of the splits, g is the gap between the rings, w is the width of both copper rings and r is the radius of the outer ring. The proposed SRR has the dimensions, in millimeters, of: $L = 10$, $d = 0.50$, $g = 0.56$, $r = 3.55$ and $w = 1.20$.

We have utilized a commercial electromagnetic solver, CST Microwave Studio, which is based on the finite integration technique. In the simulation setup, MA is illuminated by a horizontally polarized plane wave in 3–6 GHz frequency band. The plane wave propagates along $-z$ direction and the direction of the electric field vector is along the x-axis. Periodic type boundary conditions are applied along x and y-axes as shown in Fig. 1(b). MA structure which consists of 300 SRRs (i.e., 15 along x-axis and 20 along y-axis) is fabricated using printed circuit board (PCB) technique as shown in Fig. 1(c).

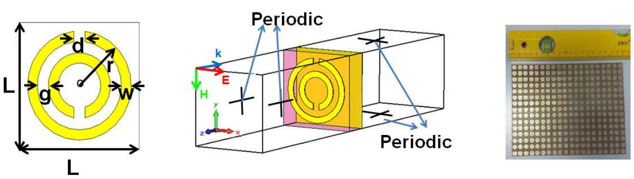

(a) (b) (c)

Figure 1: (a) Front view. (b) Perspective view of the simulation. (c) Photograph of the fabricated MA sample.

In the experimental setup, as shown in Fig. 2(a), a vector network analyzer (Rohde & Schwarz ZNB 8, 9 kHz–8.5 GHz), a pair of standard gain pyramidal horns antennas (ARRA 187-862) and a thermal imager (FLIR T650sc) are used. The distance between the horn antennas is set at 34 cm to prevent the near fields effects on the reflection and the MA is located 60 cm away from the antennas. The two horn antennas serving as the source and receiver are connected to the network analyzer by using low loss exible cables in order to measure the reflection coefficient.

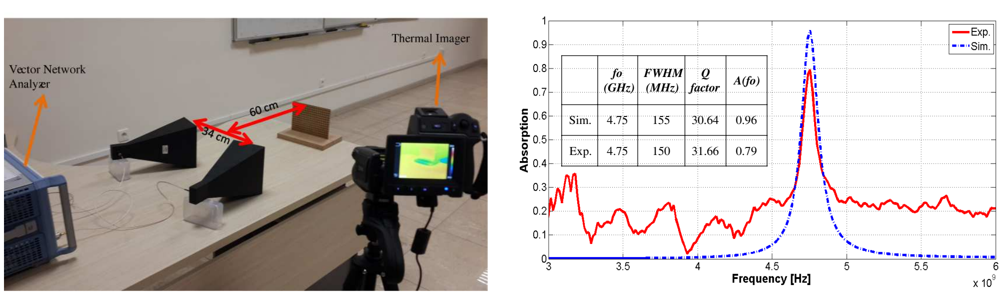

	fo (GHz)	FWHM (MHz)	Q factor	A(fo)
Sim.	4.75	155	30.64	0.96
Exp.	4.75	150	31.66	0.79

(a) (b)

Figure 2: (a) The experimental setup. (b) Simulated and measured absorption of the MA structure.

We experimentally verified the behavior of the absorber by measuring the reflectance. In order to measure standard reflection response, the back plane of the MA which is completely metallic is measured at the first phase. In the second phase, the reflection coefficient is measured by using surface of the MA which includes SRR units. The frequency dependent absorption $A(f)$ of a material is related to its transmission $T(f)$ and reflection $R(f)$ by $A(f) = 1 - T(f) - R(f)$. Here, $R(f) = |S_{11}(f)|^2$ and $T(f) = |S_{21}(f)|^2$ where $S_{11}(f)$ and $S_{21}(f)$ are reflection and transmission coefficients, respectively. $T(f)$ is zero due to the presence of the continuous copper ground plane. Thus, the total absorption is calculated only by the reflection. In order to achieve the maximum absorption, the reflection should be minimized. The frequency characteristic of the absorption is presented in Fig. 2(b). It is noted that the reflection of the absorber drops to a minimum at 4.75 GHz denoting impedance matching with the free space. We obtained simulated and measured values of 96% and 80% at 4.75 GHz, respectively. These results show that the RF simulation results are in good agreement with the measurements such that near-perfect absorption occurs at 4.75 GHz when the incident electric field vector is perpendicular to the SRR gaps. On the other hand, near-zero absorption is obtained when the incident electric field vector is parallel to the gaps. The quality-factor can be calculated from the resonance spectra in Fig. 2(b) by the following equation:

$$Q = \frac{f_0}{\Delta f_{FWHM}} \tag{1}$$

Here, f_0 is the resonance frequency and Δf_{FWHM} is its half maximum width. The Q-factor from the simulation and experimental results using Eq. (1) was found to be approximately 30.64 and 31.66, respectively.

3. ABSORBTION MECHANISM OF THE METAMATERIAL ABSORBER

Physical mechanisms of the RF absorption and the RF induced heat loss are investigated using further electromagnetic numerical simulations and thermal imaging measurement. Experiments are carried out to explore the absorbing characteristics for different polarizations of normal incident EM waves at on-resonance (4.75 GHz) and off-resonance (4.00 GHz) frequencies.

For the on-resonance and horizontal polarization case, the electric field is strongly concentrated at the outer ring split as shown in Fig. 3(a-i). However, relatively low electric field distribution is observed at the outer split region for the case of off-resonance as seen in Fig. 3(a-ii). As expected, there is negligible electric field distribution in vertical polarization case shown in Fig. 3(a-iii) and Fig. 3(a-iv), respectively.

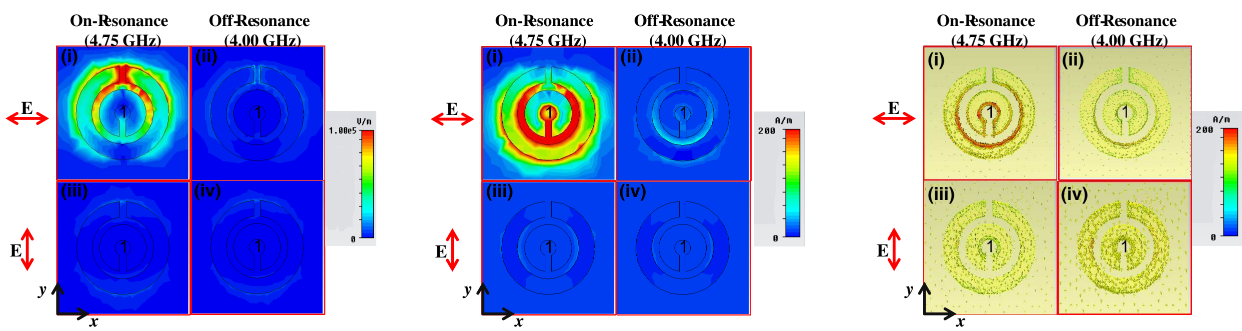

(a) (b) (c)

Figure 3: (a) Electric field distribution of the MA, $|E|$ field. (b) Magnetic field distribution of the MA, $|H|$ field. (c) Surface current distributions on the front side of the MA.

It can be observed that for the case of on-resonance and horizontal polarization, the magnetic field component is coupled to the gap and inner split as seen in Fig. 3(b-i). In case of off-resonance, relatively low magnetic field distribution is also observed at the gap region as shown in Fig. 3(b-ii). While the MA is illuminated by a vertical polarized plane wave, there is negligible magnetic field distribution as illustrated in Fig. 3(b-iii) and Fig. 3(b-iv), respectively.

Subsequently, the surface current distribution is investigated, as shown in Fig. 3(c). When the incident field is horizontally polarized, for the case of on-resonance, it is observed that the current distribution mainly focuses on the bottom side of the outer ring as seen in Fig. 3(c-i). For the case of off-resonance, the current distribution which is relatively lower than on-resonance case, is also observed as shown in Fig. 3(c-ii). When the MA is illuminated by vertically polarized field, the current is not induced over a specific part of the SRR for onand off-resonance cases as illustrated in Fig. 3(b-iii) and Fig. 3(b-iv), respectively.

The MA is illuminated by RF radiation (its frequency is between 4.74 and 4.76 GHz and power is 30 dBm) from the Vector Network Analyzer. Thermal imager is located with an angle of 10 degree to prevent the metallic reflection. Using the thermal imager, surface temperature measurement is taken before the RF power was applied. Then, the remote surface temperature is measured in the 5 minute intervals in the case of on- and off-resonances. Later, the measurements are repeated for the vertically polarized plane wave. The heat loss induced remote temperature measurements are obtained by calculating average tempereture of MA with ThermalCAM Researcher program as shown in Fig. 4. It is shown that a slight temperature difference ($\Delta T = 0.6°\text{C}$) happens with respect to the ambient temperature for the MA of the near-perfect absorption whereas the MA of the near-zero absorption has zero temperature ($\Delta T = 0°\text{C}$) difference.

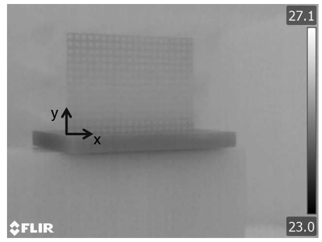

Figure 4: Thermal image of the MA.

4. CONCLUSION

In this paper, we presented the design, simulation, fabrication and RF/thermal imaging measurement of a MA having narrowband absorption resonance in the microwave region. The fabricated MA exhibits absorption peak at 4.75 GHz which is in good agreement with the simulated result. Effect of the RF induced heat loss over the front surface of the MA is investigated. Based on the remote temperature measurements using thermal imager, a slight temperature difference is observed for the MA of near-perfect absorption. Depending on these results, it is possible to say that, temperature difference of MA is linked to the RF power absorption. So, in stealth applications, the thermal effect of MAs have to be considered against remote thermal sensing systems in infrared region.

REFERENCES

1. Fang, N., H. Lee, C. Sun, and X. Zhang, "Subdiffraction-limited optical imaging with a silver superlens," *Science*, Vol. 308, No. 5721, 534–537, 2005.
2. Si, L. M. and X. Lv, "CPW-FED multi-band omni-directional planar microstrip antenna using composite metamaterial resonators for wireless communications," *Progress In Electromagnetics Research*, Vol. 83, 133–146, 2008.
3. Liu, N., M. Mesch, T. Weiss, M. Hentschel, and H. Giessen, "Infrared perfect absorber and its application as plasmonic sensor," *Nano Lett.*, Vol. 10, No. 7, 2342–2348, 2010.
4. Landy, I. N., S. Sajuyigbe, J. J. Mock, D. R. Smith, and W. J. Padilla, "Perfect metamaterial absorber," *Phys. Rev. Lett.*, Vol. 100, No. 20, 207402, 2008.
5. Li, L., Y. Yang, and C. H. Liang, "A wideangle polarization-insensitive ultra-thin metamaterial absorber with three resonant modes," *J. Appl. Phys.*, Vol. 110, 063702, 2011.
6. Veselago, V. G., "The electrodynamics of substances with simultaneously negative values of ε and μ," *Sov. Phys. Uspekhi*, Vol. 10, 509–514, 1968.
7. Zhu, B., Z. Wang, C. Huang, Y. Feng, J. Zhao, and T. Jiang, "Polarization insensitive metamaterial absorber with wide incident angle," *Progress In Electromagnetics Research*, Vol. 101, 231–239, 2011.
8. He, X. J., Y. Wang, T. L. Gui, and Q. Wu, "Dual-band terahertz metamaterial absorber with polarization insensitivity and wide angle," *Progress In Electromagnetics Research*, Vol. 115, 381–397, 2011.
9. Bian, B. R., S. B. Liu, S. Y. Wang, X. K. Kong, H. F. Zhang, B. Ma, and H. Yang, "Novel tripleband polarization-insensitive wide-angle ultra-thin microwave metamaterial absorber," *J. Appl. Phys.*, Vol. 114, No. 19, 194511, 2013.
10. Wang, B. Y., S. B. Liu, B. R. Bian, Z. W. Mao, X. C. Liu, B. Ma, and L. Chen, "A novel ultrathin and broadband microwave metamaterial absorber," *J. Appl. Phys.*, Vol. 116, 094504, 2014.
11. Pendry, J. B., A. J. Holden, D. J. Robbins, and W. J. Stewart, "Magnetism from conductors and enhanced nonlinear phenomena," *IEEE Trans. Microw. Theory Tech.*, Vol. 47, 2075–2084, 1999.